
Measuring E and B Fields in Laser-Produced Plasmas with Monoenergetic Proton Radiography

The generation of electromagnetic fields (E/B) by interactions of laser light with matter is a process of fundamental interest in high-energy-density (HED) physics.¹ The primary mechanism behind field formation is the loss of energetic electrons from the heated region, resulting in the breakdown of neutrality. Many processes can then contribute to field generation and evolution, but their relative importance depends on interaction parameters.^{1–5} For long-pulse, low-intensity laser light, the dominant source for B -field generation is noncollinear electron density and temperature gradients ($\nabla n_e \times \nabla T_e$); the dominant source for E fields is $\nabla P/n_e$, a consequence of nonuniform laser irradiation.^{1–5} For circular laser spots, the B fields have a toroidal configuration with scale length comparable to the spot size. In a regime with low Z and high temperature, where resistivity is low, B -field growth is usually linear in time and is balanced primarily by convective losses (i.e., the B field is “frozen in”).^{1–3,5} Under these circumstances, B -field evolution can be described by the Faraday equation combined with a simplified version of the generalized Ohm’s law:

$$\frac{\partial \mathbf{B}}{\partial t} \approx \nabla \times (\mathbf{v} \times \mathbf{B}) - \frac{1}{en_e} \nabla n_e \times \nabla T_e, \quad (1)$$

where \mathbf{v} is the plasma fluid velocity.

In addition to their importance to fundamental HED physics, these fields have important implications for several current problems. In inertial confinement fusion (ICF), magnetic fields (\sim MG) are generated inside a hohlraum by long-pulse (\sim 1-ns) laser illumination.^{6–8} Such fields can reduce heat flow since cross-field thermal conductivity is modified by a factor of $(1 + \omega_{ce}^2 \tau^2)^{-1}$, where ω_{ce} is the electron gyro frequency and τ is the collision time. The result is altered distributions of electron temperature and density, enhancing laser–plasma instabilities, and implosion asymmetries.^{6–8} The experiments described here are the first to directly measure fields generated by the types of laser beams used in direct- and indirect-drive ICF.

Previous work focused largely on short-pulse, high-intensity lasers,^{9–11} and field measurements were based on Faraday rotation,¹⁰ probes,⁴ or high-order laser harmonics.¹¹ It has also been

proposed that proton radiography could provide a method for measuring fields through the deflections they induce in proton trajectories; recent work by Mackinnon *et al.*¹² demonstrated that high-resolution images containing deflection information could be obtained, although no direct connections were made between images and fields. In their experiment, backlighter protons were generated by irradiating a solid tungsten target with a high-intensity petawatt laser beam (300-fs duration with an intensity of 1×10^{19} W/cm²); the result was a large proton flux and a continuous energy spectrum up to \sim 50 MeV. These protons were passed through a mesh and used to image a plasma generated by a single laser beam (300 ps) on a 120- μ m Cu wire. More recently, work by Romagnani *et al.*¹³ utilized side-on proton radiography to study the E field generated by a high-intensity (\sim 10¹⁸ W/cm²), short-pulse (\sim 1.5-ps) laser driving an Au foil; the probing proton flux had a continuous energy spectrum and was generated from a 10- μ m Au foil irradiated by an \sim 300-fs-long, 2×10^{19} W/cm² laser pulse.

A novel imaging technology has been developed that combines a monoenergetic proton backlighter with a matched detection system.^{14,15} Protons are generated as nuclear fusion products from the reaction $D + {}^3\text{He} \rightarrow \alpha + p$ in exploding-pusher implosions of D³He-filled, glass-shell capsules;¹⁶ the proton birth energy is $E_p = 14.7$ MeV with a small amount of thermal broadening. For the experiments described here, backlighter implosions were driven by 20 OMEGA laser beams; a typical measured proton spectrum is shown in Fig. 108.30, indicating a proton yield of $\sim 3 \times 10^8$. The spatial size of the proton source was measured with a proton-emission imaging system,¹⁷ which determined that the source was nearly spherical and had approximately a Gaussian radial emission profile with a full width at half maximum (FWHM) of ~ 45 μ m. The timing of the proton production was measured by a proton temporal diagnostic (PTD);¹⁸ protons were produced during an interval of ~ 150 ps, and the time of onset of the burn was adjustable. The protons were detected by a CR-39 track detector configured for imaging.¹⁵ This approach has distinct advantages over radiography with broadband proton sources (such as intense-laser-induced sources); it allows us to optimize

a special detector design and to make precise connections between particle deflections and field magnitudes.

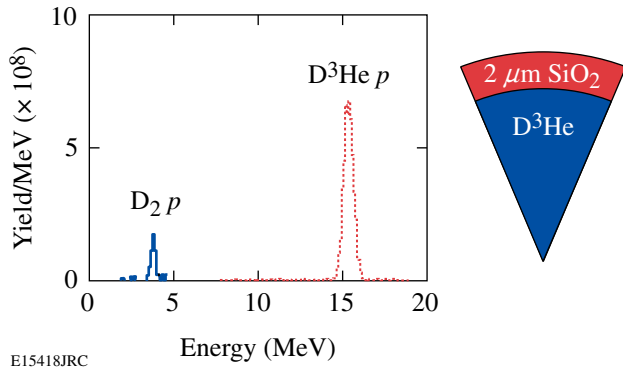


Figure 108.30

Measured energy spectra of monoenergetic D^3He and D_2 protons generated in an implosion of a thin-glass shell filled with D^3He gas (OMEGA shot 42767). The data described in this article correspond to the D^3He protons; use of the 3-MeV D_2 protons will be explored in future work.

Our experimental setup, illustrated schematically in Fig. 108.31, was designed for quantitative imaging of fields generated by the interaction of a laser with a plastic (CH) foil. In each experiment, 14.7-MeV backlighter protons were passed through meshes with 150- μm periods (to form discrete, 75- μm beamlets with ~ 2000 protons each) and used to simultaneously image two separate laser-plasma interactions: one imaged face on and the other imaged from the side. The laser-plasma interactions on each CH foil were induced by a single laser *interaction* beam with a 0.351- μm wavelength, incident 23° from the

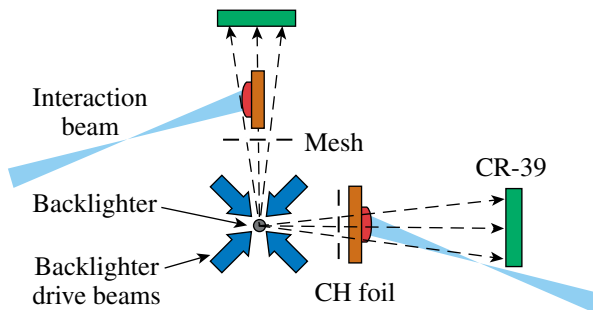


Figure 108.31

Schematic illustration of our experimental setup and the physical relationship among the proton backlighter (imploded D^3He -filled capsule), mesh, CH foils, CR-39 imaging detectors, and OMEGA laser beams, as used for simultaneous radiography of two separate laser-foil interactions (face-on and side-on). The distances of components from the backlighter were 0.8 cm for mesh, 1 cm for foil, and 36 cm for the detector.

normal direction. The laser had a square pulse either 1 ns or 0.6 ns long, with an energy of 500 J or 250 J. The diameter of the laser beam on the foil (containing 95% of the energy deposition) was determined by the phase plate,¹⁹ which was either SG2 (500 μm) or SG4 (800 μm); the resulting laser intensity was of the order of 10^{14} W/cm². X-ray emission indicates that the plasmas have $n_e \sim 10^{20}$ to 10^{22} /cm³ and $T_e \sim 1$ keV.

The interaction of the laser with the CH foil was modeled with the 2-D *LASNEX* hydrocode.²⁰ The magnetic-field package²¹ in *LASNEX* includes the full Braginskii cross-field transport model and spontaneously generates fields in the presence of nonparallel temperature and density gradients. The proton transport through these fields and plasmas was modeled with the *LSP* hybrid PIC (particle-in-cell) code.²² Because only a single energy (14.7 MeV) was used, directly comparing simulations and experimental data provides unambiguous quantitative information about fields. Simulations⁸ indicate that face-on radiography is largely sensitive only to the B field,²³ while side-on radiography is primarily sensitive only to the E field. This allows E and B fields to be measured separately.

Figure 108.32(a) shows face-on images acquired from three different shots. Laser timing was adjusted so the 14.7-MeV protons arrived at the foil at 0.0, 0.33, and 0.64 ns, respectively, after the laser interaction beam was turned on. The laser beam had an SG4 phase plate (800- μm diameter), with a 1-ns pulse and 500 J of energy. The measured images are very similar to the *LASNEX* + *LSP* simulations shown in Fig. 108.32(b), in terms of both the time dependence of the apparent diameter of the plasma bubble and the amount of distortion of the mesh pattern inside the plasma bubble region due to the magnetic lens effect. Significant distortions occurred near the border of the bubble, where the proton beamlets were deflected by a strong B field and piled up to form a sharp circular ring; smaller distortion at the center indicates a smaller, but measurable B field there. These features are largely reproduced by simulations illustrated in Fig. 108.33, showing that toroidal B fields are concentrated on a hemispherical shell surrounding the ablative plasma bubble; they have maximum amplitude near the edge but fall to zero at the center. The B fields can be estimated from the data by using the linear displacement ξ of the beamlets in an image from where they would be without the distortion, together with the geometry of the imaging system and the scale length ($L_B \equiv B/\nabla B$) in the direction perpendicular to the image ($B \propto E_p^{0.5} L_B^{-1}$). L_B was estimated to be $L_B \sim L_{\parallel} \equiv n_e/\nabla n_e$, which is about the radius of the plasma bubble. This estimated L_B is within a factor of 2 of what one would infer from the simulations near the edge of the bubble. The inferred peak B values of about 0.5 MG agree

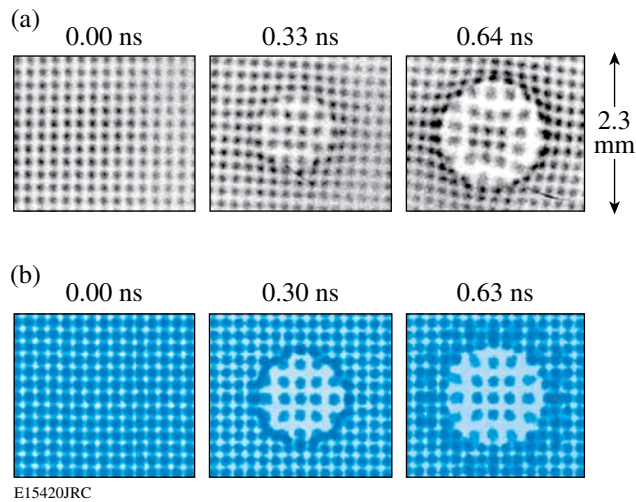


Figure 108.32

(a) Measured face-on, 14.7-MeV proton images showing the effects of the magnetic field generated by laser-plasma interactions. Each image is labeled by the time interval between the arrival at the foil of the interaction beam and the arrival of the imaging protons. The interaction beam had a 1-ns pulse length. The labeled dimensions of the image are scaled to the location of the foil. Note that the apparent 188- μm separation of beamlets in the unperturbed sections of the images corresponds to the separation at the mesh (150 μm) magnified by the ratio (source-to-foil distance)/(source-to-mesh distance). (b) Images simulated by *LASNEX* + *LSP* for the conditions that produced the experimental images shown in (a).

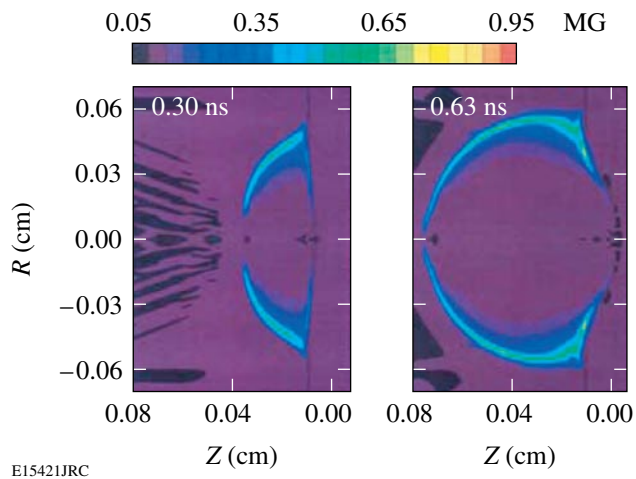


Figure 108.33

Time evolution of B -field strength on a cross section of the plasma bubble, simulated by *LASNEX* for the experimental conditions of Fig. 108.32. In each case, the horizontal coordinate z is the distance from the foil (assuming the laser is incident from the left), and the vertical coordinate R is the distance from the central axis of the plasma bubble. The largest field occurs near the surface of the plasma bubble, and the largest line integral parallel to the z direction occurs near the bubble edge.

well with simulations. In contrast to previous experiments and simulations, where the plasmas were usually generated by a short-pulse laser (~ 1 to 100 ps), we used long pulses that result in time evolution on a scale longer than our 150-ps sampling time; this allows us to clearly measure the time evolution of the field structure as shown in Fig. 108.32.

We can be more quantitative about data-simulation comparisons. The displacements ξ of individual beamlet positions in the images represents not lateral displacements at the foil but angular deflections from interactions with fields near the foil that result in lateral displacement at the detector. Angles of deflection can be inferred directly from displacements ξ by using the experiment dimensions, but quantitative comparisons between measured and simulated images are most easily made in terms of image dimensions and values of ξ . In Fig. 108.32, for example, we can look at the apparent diameter of the plasma bubbles (where beamlet “pileup” occurs). At ~ 0.3 ns it is about 1.5 mm for both simulation and data, although the value for the real image is harder to measure exactly because the pileup position is not as well defined. At ~ 0.6 ns, both data and simulation show diameters of about 1.6 mm. Next we can look at the displacements ξ in the centers of the images, which are proportional to the magnetic field in the centers of the bubbles. At ~ 0.3 ns, ξ is about 40 μm for both data and simulation, showing good agreement at that time. At 0.64 ns, the agreement is not so good since ξ is about 50 μm for the simulation but approximately zero for the data. Finally, we look outside the bubbles and see that the data show a slight mesh distortion that is not apparent in the simulations; this could suggest that the simulations underestimated the plasma resistivity, or that the interaction laser had more energy in its wings than assumed in the simulations. The simulations have done a good job of modeling the overall behavior of the plasma bubble, indicating that basic physics issues were properly addressed, but some differences merit further investigation.

Images acquired with different distributed phase plates used to condition the laser focal spots are contrasted in Fig. 108.34: SG4 for the first row (800 μm) and SG2 for the second row (500 μm). In all cases the laser pulses had similar energy and pulse shape (~ 250 J, 0.6 ns square), so the laser intensity for the second row was ~ 2.6 times higher. This resulted in deflection of the central beamlets by nearly a factor of 10 more in the central region for SG2 than for SG4 at ~ 0.4 ns, but not at ~ 0.7 ns. This is consistent with our *LASNEX* simulations, which show that a significant B field is generated in the central region at earlier times, but moves to the edge of the plasma because of plasma expansion.

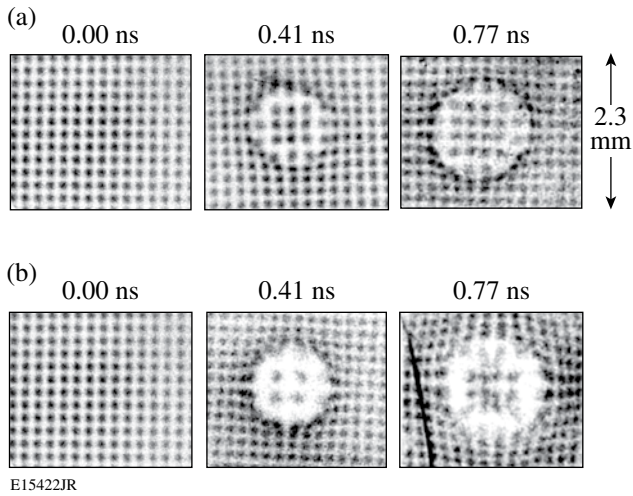


Figure 108.34
 14.7-MeV-proton radiographs recorded for experiments with a similar interaction laser pulse (~ 0.6 ns square, ~ 250 J) but different phase plates: (a) SG4 and (b) SG2. The smaller diameter of the SG2 beam resulted in an intensity ~ 2.6 times higher than SG4, causing greatly increased image distortion.

The images shown in Fig. 108.35 show a consequence of using no phase plate for the interaction beam. Both images were recorded around 0.3 ns and utilized similar interaction beam diameters, pulse shapes, and laser energy. Compared to the image recorded with phase plate (a), the image recorded without (b) shows a more-chaotic pattern, implying a B field with medium-scale structure (at $\sim 20\%$ to 30% of the bubble size). This observation is consistent with theoretical expectations. An unconditioned OMEGA laser beam has nonuniformities at scales of $\sim 40 \mu\text{m}$. This can lead to medium-scale, random

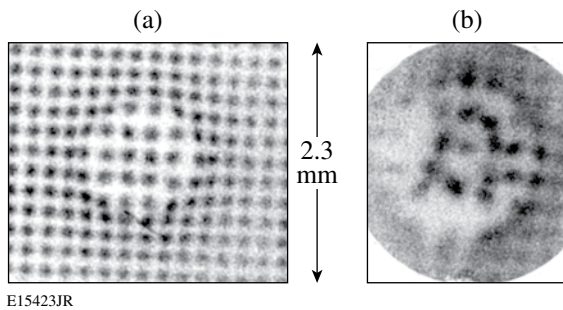


Figure 108.35
 Effects of phase plates on the B -field structure are demonstrated by 14.7-MeV proton radiographs made by using interaction beams (a) with and (b) without phase plates under conditions otherwise similar. [Image (b) is from an earlier experiment in which the field of view was smaller and the outer (gray) part of the imaged area was covered by a $70\text{-}\mu\text{m}$ mylar washer.] Chaotic structure is clearly seen in image (b).

plasma structures, in particular those associated with very localized regions of strong $\nabla n_e \times \nabla T_e$, including the resonance absorptions at local oblique incidence, filaments, laser hot spots, and instabilities.^{1–5} When phase plates are used, they convert the medium-scale laser nonuniformities to a smaller scale of $\sim 2 \mu\text{m}$ (the speckle size). Short-wavelength plasma structures are more easily smoothed by thermal transport than medium-wavelength structures, so plasmas are more uniform when phase plates are deployed.

Side-on measured (a) and simulated (b) images are shown in Fig. 108.36 for the same shot that generated the center image shown in Fig. 108.34(b). The displacements of the beamlets away from the foil represent the effect of the electric field generated by $\nabla P/n_e$. The size of the apparent beamlet displacement ($\xi \approx 60 \mu\text{m}$) is used to estimate the E -field strength ($E \propto \xi E_p L_\perp^{-1}$); by assuming that the field operates over a scale length L_\perp comparable to the radius of the plasma bubble, $E \approx 1.5 \times 10^8$ V/m was deduced. The magnitude of the beamlet displacement in the experiment is very similar to what is seen in the simulation.

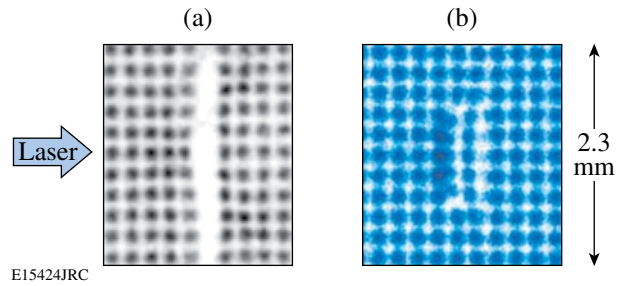


Figure 108.36
 (a) Data and (b) simulation for the side-on images. The distortion in the center column of (a) resulted from the E field. The large separation between the two center columns of beamlets in (a) is due to attenuation by the CH foil, which is $50 \mu\text{m}$ thick but 3 mm long in the direction parallel to the proton trajectories. This effect is not seen in (b) because proton-foil interactions were not modeled in the LSP simulation. The magnitude of the beamlet displacement in the experiment is very similar to what is seen in the simulation.

In summary, we studied electromagnetic fields generated by the interaction with plasmas of long-pulse, low-intensity laser beams that are particularly relevant to inertial confinement fusion experiments. The field strengths have been measured using novel monoenergetic proton radiography methods. High-resolution, time-gated radiography images of a plastic foil driven by a 10^{14}-W/cm^2 laser implied B fields of ~ 0.5 MG and E fields of $\sim 1.5 \times 10^8$ V/m. The experiments also demonstrated the smoothing effects of laser phase plates by showing that they substantially reduce medium-scale chaotic field structure.

Overall, there was good agreement between experiment and *LASNEX + LSP* simulations, as demonstrated here for the first time, although there exist intriguing differences that merit further investigation. In addition, experiments and simulations, soon to be conducted, will carefully study late times in the evolution of the field structure and probe structures for which the 2-D symmetry implicit in the *LASNEX + LSP* simulations will be broken.

ACKNOWLEDGMENT

The work described here was performed in part at the LLE National Laser Users' Facility (NLUF) and was supported in part by the U.S. DOE (Grant No. DE-FG03-03SF22691), LLNL (subcontract Grant No. B504974), and LLE (subcontract Grant No. 412160-001G).

REFERENCES

1. S. Eliezer, *The Interaction of High-Power Lasers with Plasmas* (Institute of Physics Publishing, Bristol, England, 2002).
2. L. Spitzer, *Physics of Fully Ionized Gases*, 2nd rev. ed., Interscience Tracts on Physics and Astronomy (Interscience, New York, 1962).
3. S. I. Braginskii, in *Reviews of Plasma Physics*, edited by Acad. M. A. Leontovich (Consultants Bureau, New York, 1965), Vol. 1, p. 205.
4. J. A. Stamper *et al.*, Phys. Rev. Lett. **26**, 1012 (1971); D. G. Colombant and N. K. Winsor, Phys. Rev. Lett. **38**, 697 (1977).
5. M. G. Haines, Phys. Rev. Lett. **78**, 254 (1997).
6. S. H. Glenzer *et al.*, Phys. Rev. Lett. **87**, 045002 (2001).
7. P. Amendt *et al.*, Bull. Am. Phys. Soc. **49**, 26 (2004).
8. R. P. J. Town *et al.*, Bull. Am. Phys. Soc. **50**, 123 (2005).
9. M. A. Yates *et al.*, Phys. Rev. Lett. **49**, 1702 (1982).
10. M. Borghesi *et al.*, Phys. Rev. Lett. **81**, 112 (1998).
11. U. Wagner *et al.*, Phys. Rev. E **70**, 026401 (2004).
12. A. J. Mackinnon, P. K. Patel, R. P. Town, M. J. Edwards, T. Phillips, S. C. Lerner, D. W. Price, D. Hicks, M. H. Key, S. Hatchett, S. C. Wilks, M. Borghesi, L. Romagnani, S. Kar, T. Toncian, G. Pretzler, O. Willi, M. Koenig, E. Martinolli, S. Lepape, A. Benuzzi-Mounaix, P. Audebert, J. C. Gauthier, J. King, R. Snavely, R. R. Freeman, and T. Boehly, Rev. Sci. Instrum. **75**, 3531 (2004).
13. L. Romagnani *et al.*, Phys. Rev. Lett. **95**, 195001 (2005).
14. C. K. Li, F. H. Séguin, J. A. Frenje, J. R. Rygg, R. D. Petrasso, R. P. J. Town, P. A. Amendt, S. P. Hatchett, O. L. Landen, A. J. Mackinnon, P. K. Patel, V. Smalyuk, J. P. Knauer, T. C. Sangster, and C. Stoeckl, Rev. Sci. Instrum. **77**, 10E725 (2006).
15. F. H. Séguin, J. A. Frenje, C. K. Li, D. G. Hicks, S. Kurebayashi, J. R. Rygg, B.-E. Schwartz, R. D. Petrasso, S. Roberts, J. M. Soures, D. D. Meyerhofer, T. C. Sangster, J. P. Knauer, C. Sorce, V. Yu. Glebov, C. Stoeckl, T. W. Phillips, R. J. Leeper, K. Fletcher, and S. Padalino, Rev. Sci. Instrum. **74**, 975 (2003).
16. C. K. Li, D. G. Hicks, F. H. Séguin, J. A. Frenje, R. D. Petrasso, J. M. Soures, P. B. Radha, V. Yu. Glebov, C. Stoeckl, D. R. Harding, J. P. Knauer, R. L. Kremens, F. J. Marshall, D. D. Meyerhofer, S. Skupsky, S. Roberts, C. Sorce, T. C. Sangster, T. W. Phillips, M. D. Cable, and R. J. Leeper, Phys. Plasmas **7**, 2578 (2000).
17. F. H. Séguin, J. L. DeCiantis, J. A. Frenje, S. Kurebayashi, C. K. Li, J. R. Rygg, C. Chen, V. Berube, B. E. Schwartz, R. D. Petrasso, V. A. Smalyuk, F. J. Marshall, J. P. Knauer, J. A. Delettrez, P. W. McKenty, D. D. Meyerhofer, S. Roberts, T. C. Sangster, K. Mikaelian, and H. S. Park, Rev. Sci. Instrum. **75**, 3520 (2004).
18. J. A. Frenje, C. K. Li, F. H. Séguin, J. DeCiantis, S. Kurebayashi, J. R. Rygg, R. D. Petrasso, J. Delettrez, V. Yu. Glebov, C. Stoeckl, F. J. Marshall, D. D. Meyerhofer, T. C. Sangster, V. A. Smalyuk, and J. M. Soures, Phys. Plasmas **11**, 2798 (2004).
19. Y. Lin, T. J. Kessler, and G. N. Lawrence, Opt. Lett. **20**, 764 (1995).
20. G. B. Zimmerman and W. L. Kruer, Comments Plasma Phys. Control. Fusion **2**, 51 (1975).
21. P. D. Nielsen and G. B. Zimmerman, Lawrence Livermore National Laboratory, Livermore, CA, UCRL-53123 (1981).
22. D. R. Welch *et al.*, Nucl. Instrum. Methods Phys. Res. A **464**, 134 (2001).
23. In addition, *E* fields can be eliminated as a cause of deflections in face-on images by utilizing, in part, the monoenergetic character of the protons to show that, on the picosecond timescale, electrons would short out the *E* fields that would be required to create the circular patterns.